Nuclear Engineering and Design xxx (2016) xxx–xxx

Contents lists available at ScienceDirect

Nuclear Engineering and Design

journal homepage: www.elsevier.com/locate/nucengdes

Large eddy simulation of a buoyancy-aided flow in a non-uniform channel – Buoyancy effects on large flow structures

Y. Duan [a,b], S. He [a,*]

[a] Department of Mechanical Engineering, University of Sheffield, Sheffield S1 3JD, UK
[b] School of Mechanical, Aerospace and Civil Engineering, University of Manchester, Manchester M13 9PL, UK

HIGHLIGHTS

- Buoyancy may greatly redistribute the flow in a non-uniform channel.
- Flow structures in the narrow gap are greatly changed when buoyancy is strong.
- Large flow structures exist in wider gap, which is enhanced when heat is strong.
- Buoyancy reduces mixing factor caused by large flow structures in narrow gap.

ARTICLE INFO

Article history:
Received 26 January 2016
Received in revised form 6 April 2016
Accepted 8 May 2016
Available online xxxx

ABSTRACT

It has been a long time since the 'abnormal' turbulent intensity distribution and high inter-sub-channel mixing rates were observed in the vicinity of the narrow gaps formed by the fuel rods in nuclear reactors. The extraordinary flow behaviour was first described as periodic flow structures by Hooper and Rehme (1984). Since then, the existences of large flow structures were demonstrated by many researchers in various non-uniform flow channels. It has been proved by many authors that the Strouhal number of the flow structure in the isothermal flow is dependent on the size of the narrow gap, not the Reynolds number once it is sufficiently large. This paper reports a numerical investigation on the effect of buoyancy on the large flow structures. A buoyancy-aided flow in a tightly-packed rod-bundle-like channel is modelled using large eddy simulation (LES) together with the Boussinesq approximation. The behaviour of the large flow structures in the gaps of the flow passage are studied using instantaneous flow fields, spectrum analysis and correlation analysis. It is found that the non-uniform buoyancy force in the cross section of the flow channel may greatly redistribute the velocity field once the overall buoyancy force is sufficiently strong, and consequently modify the large flow structures. The temporal and axial spatial scales of the large flow structures are influenced by buoyancy in a way similar to that turbulence is influenced. These scales reduce when the flow is laminarised, but start increasing in the turbulence regeneration region. The spanwise scale of the flow structures in the narrow gap remains more or less the same when the buoyancy parameter is smaller than a critical value, but otherwise it reduces visibly. Furthermore, the mixing factors between the channels due to the large flow structures in the narrow gap are, generally speaking, reduced by buoyancy.

1. Introduction

Rod bundles are a typical geometry configuration of the fuel assemblies in many nuclear reactors. The coolant flows through the sub-channels formed by arrays of fuel rods (or pins). Such sub-channels are connected to each other through 'narrow' gaps of continuously varying sizes, which are characterised by the non-dimensional pitch-to-diameter ratio. Soon after the first generation of nuclear reactors was integrated into the electricity grid, the unusual turbulent intensity and higher than expected inter-channel mixing rates were discovered to exist in the narrow gap region.

Before Hooper and Rehme (1984), researchers used to believe that such unexpected behaviours of the flow assemblies were due to the strong secondary flow in the channels (refers to Ouma and Tavoularis, 1991; Guellouz and Tavoularis, 1992; Meyer, 2010). Hooper and Rehme (1984) first demonstrated the existence of the energetic and almost periodic flow structures in the vicinity of narrow gaps formed by the rods. They suggested that the flow

* Corresponding author.
E-mail address: s.he@sheffield.ac.uk (S. He).

http://dx.doi.org/10.1016/j.nucengdes.2016.05.007
0029-5493/

Nomenclature

Roman symbols

Bo^*	buoyancy parameter, $Bo^* = Gr^*/(Re^{3.425}Pr^{0.8})$
D	diameter of the rod
D_h	hydraulic diameter
f	frequency
f_p	dominant frequency of the flow structures in the channel
Gr^*	Grashof number based on heat flux, $g\beta D_h^4 q/\lambda\upsilon^2$
Nu	Nusselt number, hD_h/λ
P/D	pitch to diameter ratio
Re	Reynolds number, $U_b D_h/\upsilon$
S	the size of the narrow gap
s	the LES quality criteria proposed by Geurts and Fröhlich (2002), defined as $s \simeq \langle\mu_{sgs}\rangle/(\langle\mu_{sgs}\rangle + \langle\mu\rangle)$
s^*	parameter in the LES quality criteria proposed by Celik et al. (2005), defined as $s^* = (\langle\mu_{sgs}\rangle + \langle\mu_{num}\rangle)/(\langle\mu_{sgs}\rangle + \langle\mu_{num}\rangle + \langle\mu\rangle)$
$St = fD_h/u$	Strouhal number
$St_\tau = fD_h/u_\tau$	Strouhal number based on u_τ
$St_b = fD_h/U_b$	Strouhal number based on U_b
St_f	the St_b of the flow structures in the forced convection case, namely Case 1
U_c	convection velocity of the Flow Structures in the narrow gap
U_b	bulk velocity
U, V and W	instantaneous velocity components in Cartesian coordinates
u', v' and w'	fluctuating velocity component
u_{eff}	effective mixing velocity between sub channels
x, y, z	spanwise direction, wall normal direction and streamwise direction
Y	the mixing ratio
Y_f	the mixing ratio in force convection case, namely Case 1

Greek symbols

δ_{ij}	distance between two subchannels
λ	wave length of the flow structures in the narrow gap or thermal conductivity
μ	dynamic viscosity
μ_{num}	numerical viscosity
μ_{sgs}	sub-grid scale viscosity
υ	kinetic viscosity, μ/ρ

Acronyms

CFL	Courant–Friedrichs–Lewy condition or number
LES	large eddy simulation
LES_IQ_v	the LES quality criteria proposed by Celik et al. (2005)
PSDX	power spectral density of u'
RANS	Reynolds-averaged Navier–Stokes
URANS	unsteady Reynolds-averaged Navier–Stokes
WALE	wall adapting local eddy viscosity sub-scale model

structures are the reasons for the high turbulent intensity in the region. They also claimed that the size of the flow structures were dependent on the size of the narrow gap. The existence of the flow structures was again proved by Möller (1991, 1992) in other experiments. The pronounced peak was shown in the power spectral density (PSD) of the spanwise velocity at the centre of the narrow gap. Also, it was suggested that the Strouhal number ($St_\tau = f_p D_h/u_\tau$) of the flow structures is only dependent on the non-dimensional gap size (S/D). In the experimental investigations of the fully developed flow in a 37-rod bundle with different pitch-to-diameter ratios, Meyer (1994) and Krauss and Meyer (1996, 1998) proved that the flow structures in the adjacent narrow gaps in the fuel assembly are strongly correlated to each other, which was also observed in the experiments by Baratto et al. (2006).

The flow instability mentioned above does not just exist in the rod bundles but also in other non-uniform flow channels, such as a trapezoid/rectangular channel with a rod mounted in it (Wu and Trupp, 1993, 1994; Guellouz and Tavoularis, 2000a,b), channels containing/connected by a narrow gap (Meyer and Rehme, 1994, 1995; Home and Lightstone, 2014) or the eccentric annular channels with a high eccentricity (Gosset and Tavoularis, 2006; Piot and Tavoularis, 2011; Choueiri and Tavoularis, 2014). In the articles by Meyer and Rehme (1994, 1995), it is shown that the structures can be presented in the flow of a wide range of Re. The large flow structures was observed in the flow with Re as low as 2300. Gosset and Tavoularis (2006) further approved that the flow structures even exist in a laminar flow, and there is a critical Re for the existence of the flow structures. In the meantime, the Strouhal number (St) of the flow structure decrease with the increase of the flow Reynolds number at initially. It is only dependent on the non-dimensional gap size once the Reynolds number is sufficiently high.

In addition to experiments, the CFD simulations are another widely used methodology to study the flows nowadays. The first attempt to use the CFD method to study flow structures in the non-uniformly geometry is dated back to late 1990s (Meyer, 2010). Most of the works were done by using the RANS/URANS method. Few authors also used the large eddy simulation to study the flow structures. It is demonstrated by many authors that the RANS method cannot accurately predict the high turbulence intensity in the narrow gap of the fuel assembly when the P/D is smaller than 1.1 (In et al., 2004; Baglietto and Ninokata, 2005; Baglietto et al., 2006 and Chang and Tavoularis, 2012). This is simply because that the steady RANS model cannot capture the inherently unsteady large flow structures in the narrow gaps.

The team led by Tavoularis in the University of Ottawa not only carried out experimental studies to investigate the coherent flow structures in the gap regions, but also devoted many efforts to study the flow structures numerically. Chang and Tavoularis (2005, 2006, 2008, 2012) investigated the fully developed flow in the geometry similar to the channel considered in Guellouz and Tavoularis (2000a,b). Due to the existence of the large flow structure, a strong oscillation of the flow temperature in the narrow gap was reported in the Chang and Tavoularis (2006). Unsteady RANS with a standard Reynolds stress turbulence model was used to simulate the fully developed flow in a 60° sector of the 37-rod bundle by Chang and Tavoularis (2007). The results agreed with the finding by Krauss and Meyer (1996, 1998) that the flow structures in the adjacent narrow gap in rod bundles are highly correlated with each other. Furthermore, it was pointed out in the article (Chang and Tavoularis, 2012) that the St of the flow structure is smaller in the developing flow region than in the fully developed region, which was proved in the experiment by Choueiri and Tavoularis (2014). It was also demonstrated that the LES is a most robust CFD methodology to study the behaviours of the flow structures, while the URANS can also reproduce the flow structures with reasonable accuracy no matter what turbulence models were chosen. It was supported by other authors'

Please cite this article in press as: Duan, Y., He, S. Large eddy simulation of a buoyancy-aided flow in a non-uniform channel – Buoyancy effects on large flow structures. Nucl. Eng. Des. (2016), http://dx.doi.org/10.1016/j.nucengdes.2016.05.007

work such as, Biemüller et al. (1996), Home et al. (2009), Home and Lightstone (2014), Merzari and Ninokata (2009), Abbasian et al. (2010), Liu and Ishiwatari (2011, 2013).

A research group in Tokyo Institute of Technology has also conducted a series of work on this topic. Their work can be found in Baglietto and Ninokata (2005), Baglietto et al. (2006), Merzari and Ninokata (2008, 2009), Merzari et al. (2008, 2009) as well as Ninokata et al. (2009). They also showed that the URANS method is reliable to predict the key characteristics of the coherent flow structures in the narrow gap of the non-uniform geometry. Nevertheless it has been shown that with no doubt the LES has an even better capacity to shown such unsteady flow structures, which can be close to the performance of the DNS, as shown in Merzari and Ninokata (2009) and Ninokata et al. (2009). Except for emphasising the strong relationship between the existence of the large flow structure and the gap size, it was shown in Merzari and Ninokata (2008) that the flow structure becomes less dominant when the Reynolds number increases. They also observed the interactions of coherent structures in adjacent sub-channels.

It is known that the buoyancy is unavoidable in the real world, e.g. in various conditions of a nuclear reactor. But the effect of the buoyancy on the unsteady flow structures has not been taken into consideration in previous studies. Due to the non-uniformity of the geometry, the strength of the buoyancy force at different parts of the flow passage may be different, which may result in a redistribution of the velocity in the geometry. Consequently, the behaviour of the coherent flow structures in the narrow gap may be changed as well. The main objective of this paper is to report an investigation of the buoyancy effect on the behaviour of large flow structures in a rod-bundle-like geometry using large eddy simulation (LES).

2. Methodology

2.1. Geometry considered

A trapezoid channel enclosing a rod in it is considered in the study. This is the same as the channel studied experimentally by Wu and Trupp (1993). As illustrated in Fig. 1, the channel contains a narrow gap close to bottom edge and a wide gap at the opposite side of the rod. The two gaps connect via the main channels which are located both sides of the rod. The diameter of rod D is 0.0508 m, the size of the narrow gap S is 0.004 m, and consequently, the ratio S/D is 0.079. The lengths of the two trapezoid bases are 0.0548 m and 0.127 m, while the height is 0.066 m. Overall, the hydraulic diameter D_h of channel is 0.0314 m. A relative short computing domain (10 D_h) is considered here with the periodic boundary condition applied to the inlet and outlet to simulate an axially fully developed condition as explained in the next sub-section.

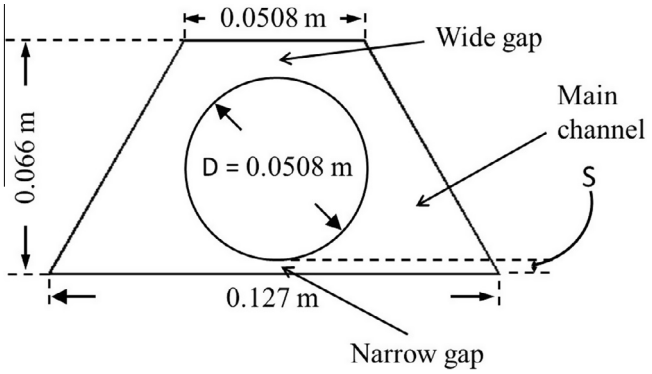

Fig. 1. A sketch of the considered geometry.

2.2. Simulation models and numerical details

Four cases have been considered to study the effect of various buoyancy forces on the behaviour of the large flow structures. The first (Case 1) is a forced convection case, while the following three (Cases 2–4) are mixed convection (buoyancy aided flow). In all of the cases, an air-like fluid at the atmosphere pressure ascends in the channel with a bulk velocity (U_b) of 2.45 m/s. The density, specific heat, thermal conductivity, and viscosity of the fluid are 1.225 kg/m^3, 1006.42 J/kg·K, 0.0242 w/m·K and 1.7894e^{-5} kg/m·s, respectively. The mass flow rate and Reynolds number are 0.11527 kg/s and 5270, respectively. The Boussinesq approximation is utilised to represent the effect of the buoyancy force. The expansion coefficient β is 0.001$\frac{1}{k}$ in all of the cases. The gravity acceleration is set to −9.8 m/s^2 in the mixed convection cases, but 0 m/s^2 in Case 1. A constant wall temperature is applied in the case (800 k, 650 k, 1427 k and 6250 k in Cases 1, 2, 3, and 4 respectively). The resultant buoyancy parameter Bo^* (proposed by Jackson et al., 1989) are 0, 1.5×10^{-6}, 2.4×10^{-6} and 1.7×10^{-5} in the cases, respectively. In order to achieve sufficiently high values of buoyancy parameter that might be encountered in the reactor (e.g., Cases 3 and 4), the wall temperatures employed appear to be unrealistically high due to the use of air at atmospheric pressure. But the absolute values of temperatures are of no significance and should not be directly compared with reactor conditions. The flow simulations are performed using large eddy simulation (LES) with the wall adapting local eddy viscosity (WALE) SGS model in Fluent 14.5. Thanks to the assumption of constant fluid properties and the use of the Boussinesq approximation for buoyancy force, the flow may be fully developed downstream of the fuel channel, which is the condition studied herein. As a result, a periodic boundary condition is applied at the inlet and outlet for both the flow and thermal fields. For the latter, under a constant-wall-temperature boundary condition, the strategy used in Fluent is to solve a non-dimensional temperature based on the following scaling (Patankar et al., 1977; Fluent, 2009):

$$\theta = \frac{T(\vec{r}) - T_{wall}}{T_{bulk,inlet} - T_{wall}} \tag{1}$$

where $T_{bulk,inlet}$ is the bulk temperature at the inlet of the computational domain. The use of a periodic boundary condition is a popular method in mixed convection studies; see for example, Kasagi and Nishimur (1997), and Piller (2005), Keshmiri et al. (2012).

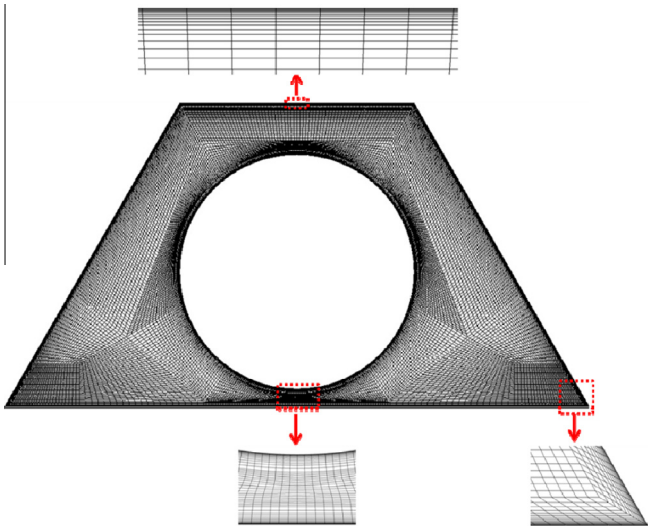

Fig. 2. An overview of the mesh.

Please cite this article in press as: Duan, Y., He, S. Large eddy simulation of a buoyancy-aided flow in a non-uniform channel – Buoyancy effects on large flow structures. Nucl. Eng. Des. (2016), http://dx.doi.org/10.1016/j.nucengdes.2016.05.007

A relatively fine mesh is required to resolve the near wall flow. To reduce the total numbers of the mesh elements, a non-uniform mesh is generated. The mesh size is small in the near wall region but bigger in the region away from walls. An overview of the mesh can be seen in Fig. 2. The first near wall mesh nodes are in the range of $5 \leqslant x^+ \leqslant 17$, $0.13 \leqslant y^+ \leqslant 0.2$ and $10 \leqslant z^+ \leqslant 16$, while y^+, x^+ and z^+ are the non-dimensional size of mesh in wall normal, spanwise and streamwise direction. There are at least 15 cells located between the wall and $y^+ = 20$, (counted in Case 1). The total number of the mesh elements is 7.8 million. The time interval of each step is 0.0001 s in all the cases, with a CFL number of ~0.2.

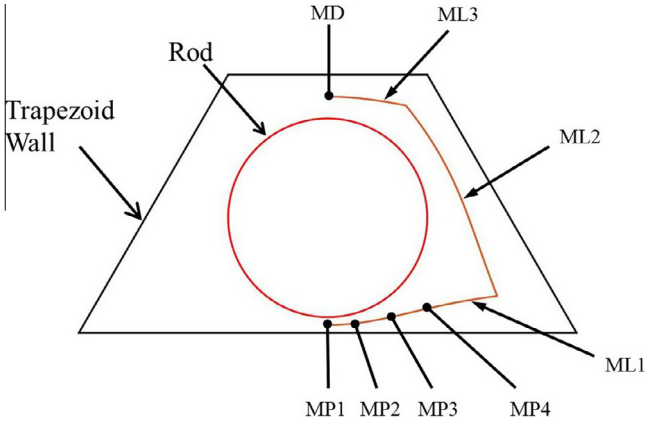

Fig. 3. Illustrations of locations as which results are shown.

To reduce the numerical dissipation, the momentum equations are solved using the *bounded central differencing* scheme; the *second order upwind* scheme is applied to solve the energy equation, while the *bounded second order implicit* method is used to solve the transient component. The *SIMPLE* scheme is used for the pressure–velocity coupling.

2.3. Locations used to extract the results

Before discussing the results, it is necessary to introduce the locations and lines used to present the results. The lines, 'ML1', 'ML2', and 'ML3', shown in Fig. 3 are used to present velocity profiles in the various regions of the flow channel. They are the equal distance lines between the rod and the trapezoid channel wall. The history of the instantaneous velocity at points such as 'MP1' and 'MD', seeing Fig. 3, are recorded for the spectrum and correlation analyses. The instantaneous velocities are also recorded at 30 points horizontally located along the line 'ML1'. Similarly, velocity is also recorded along 'MP1' and 'MD', but at different axial locations.

3. Results and discussion

3.1. The quality of the simulations

Since there is a lack of experimental or DNS data under the conditions concerned herein, the LES quality criteria suggested in Geurts and Fröhlich (2002) and Celik et al. (2005, 2009) are used to assess the quality of the results. It was suggested by

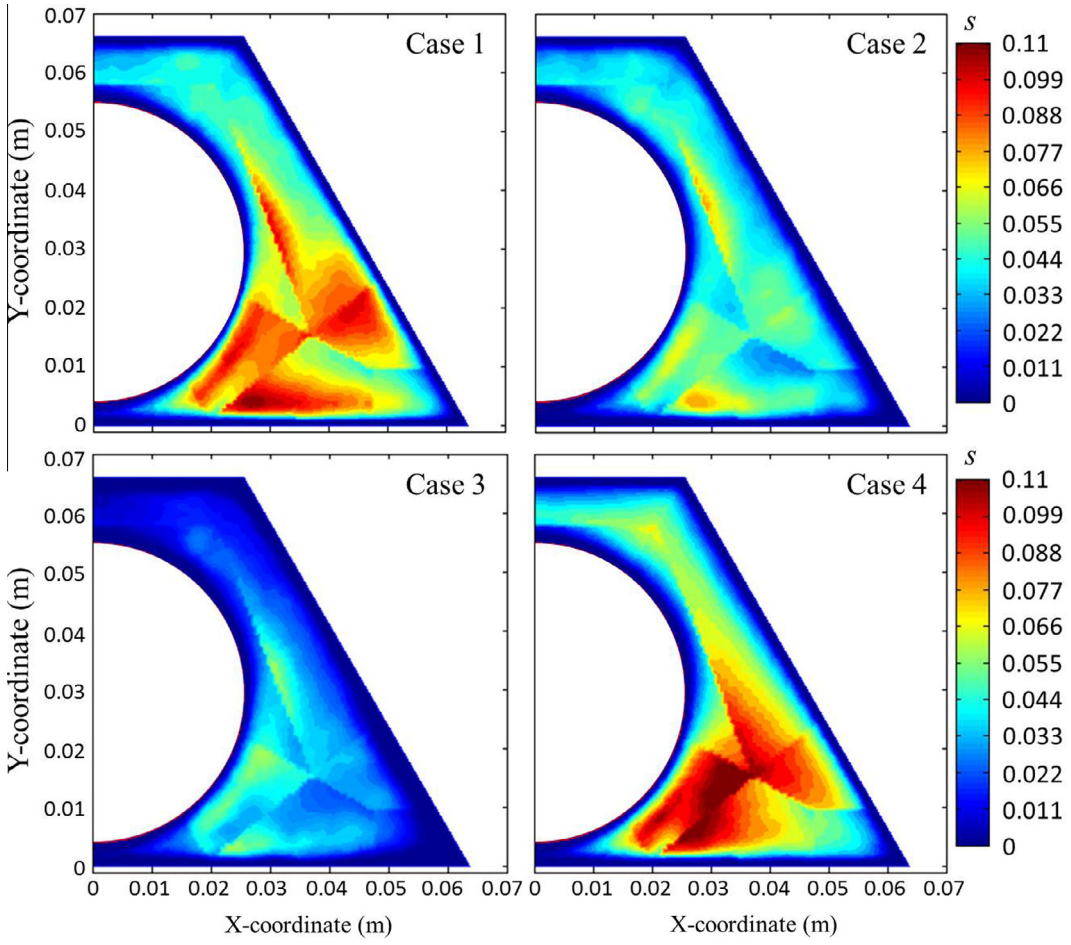

Fig. 4. Large eddy simulation quality criteria *s*.

Please cite this article in press as: Duan, Y., He, S. Large eddy simulation of a buoyancy-aided flow in a non-uniform channel – Buoyancy effects on large flow structures. Nucl. Eng. Des. (2016), http://dx.doi.org/10.1016/j.nucengdes.2016.05.007

Geurts and Fröhlich (2002) that the quality of the LES simulation can be assessed by considering the ratio of the turbulent dissipation and the total dissipation, which can be estimated by $s \simeq \frac{\langle \mu_{sgs} \rangle}{\langle \mu_{sgs} \rangle + \langle \mu \rangle}$, see Celik et al. (2005). The LES result is considered to be more like DNS when s approaches 0. Another option is to use $\text{LES\_IQ}_v = \frac{1}{1+\alpha_v \left(\frac{s^*}{1-s^*}\right)^n}$ proposed by Celik et al. (2005), where $s^* = \frac{\langle \mu_{sgs} \rangle + \langle \mu_{num} \rangle}{\langle \mu_{sgs} \rangle + \langle \mu_{num} \rangle + \langle \mu \rangle}$. In this approach, when LES_IQ_v is closer to 1, the LES simulation is more like a DNS simulation. It is suggested in Celik et al. (2009) that μ_{num} can be approximated by μ_{sgs}.

Figs. 4 and 5 show contours of the different criteria. Due to the symmetry of the geometry, the figures only show the left part of the channel. Since both of criteria consider the μ_{sgs}, which is a function of the mesh element's size, the values of the criteria are directly related to the size of the mesh elements. The contours of the criteria in the channel reflect the non-uniform distribution of the mesh in the region. As shown in Fig. 4, the values of s are very low (close to 0) in the near well region, while the values of s are ~0.11 in the main channel. It should be reminded that s stand for the fraction of the turbulence kinetic energy modelled by the LES. As Pope (2000) pointed out a good LES simulation should resolve over 80% of the turbulence kinetic energy. Using the criteria, it can be seen that the simulations are of very high quality. Further, the values of LES_IQ_v approach 1 in the near wall region and ~0.97 in the main channel, which also demonstrates the high quality of the simulations, see Fig. 5.

3.2. Flow pattern

3.2.1. Statistics of the velocity field

The contours of the mean streamwise velocity distribution in various cases are presented in Fig. 6. As illustrated in the figure, the velocity magnitude in the forced convection case (Case 1) decreases as the flow passage becomes narrower. But this pattern is significantly modified in the buoyancy influenced cases. The location of the maximum velocity is moved to the top corner of the channel in Case 2. With the increases of buoyancy force in Case 3, the high velocity patch expands towards the main channel and the centre of wide gap. The maximum velocity is located in the narrow gap and the bottom corner in Case 4, where the buoyancy force is the strongest. This observation is similar to the result obtained by Forooghi et al. (2015).

The velocity profiles on the equal-distance lines 'ML1', 'ML2' and 'ML3' are illustrated in the Fig. 7. The velocity increases from the centre of the narrow gap (the beginning of the line, 0 m) and reaches a maximum towards the end of 'ML1' in Cases 1–3, while the trend is totally reversed in Case 4. The maximum velocity is in the centre of the narrow gap in Case 4, while the minimum value on 'ML1' can be found near the centre of the main channel. Different from the reducing trend of the velocity observed along 'ML2' in Case 1, it increases in Cases 2 and 3 and shows a 'U' profile in Case 4. These are consistent with the observations in the contours. The velocity on 'ML3' in Cases 2 and 3 is higher than it in Case 1, while the lowest occurs in Case 4. The redistribution of the velocity field

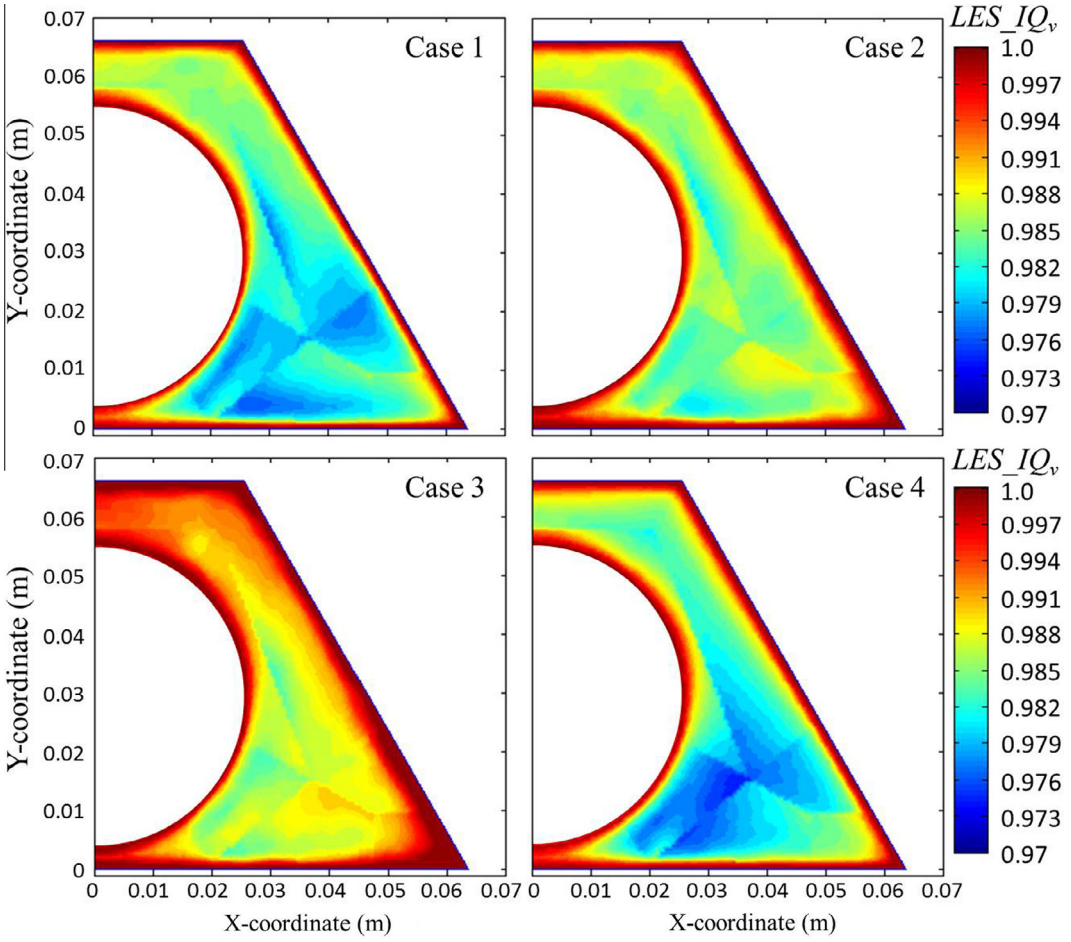

Fig. 5. Large eddy simulation quality criteria LES_IQ_v.

Please cite this article in press as: Duan, Y., He, S. Large eddy simulation of a buoyancy-aided flow in a non-uniform channel – Buoyancy effects on large flow structures. Nucl. Eng. Des. (2016), http://dx.doi.org/10.1016/j.nucengdes.2016.05.007

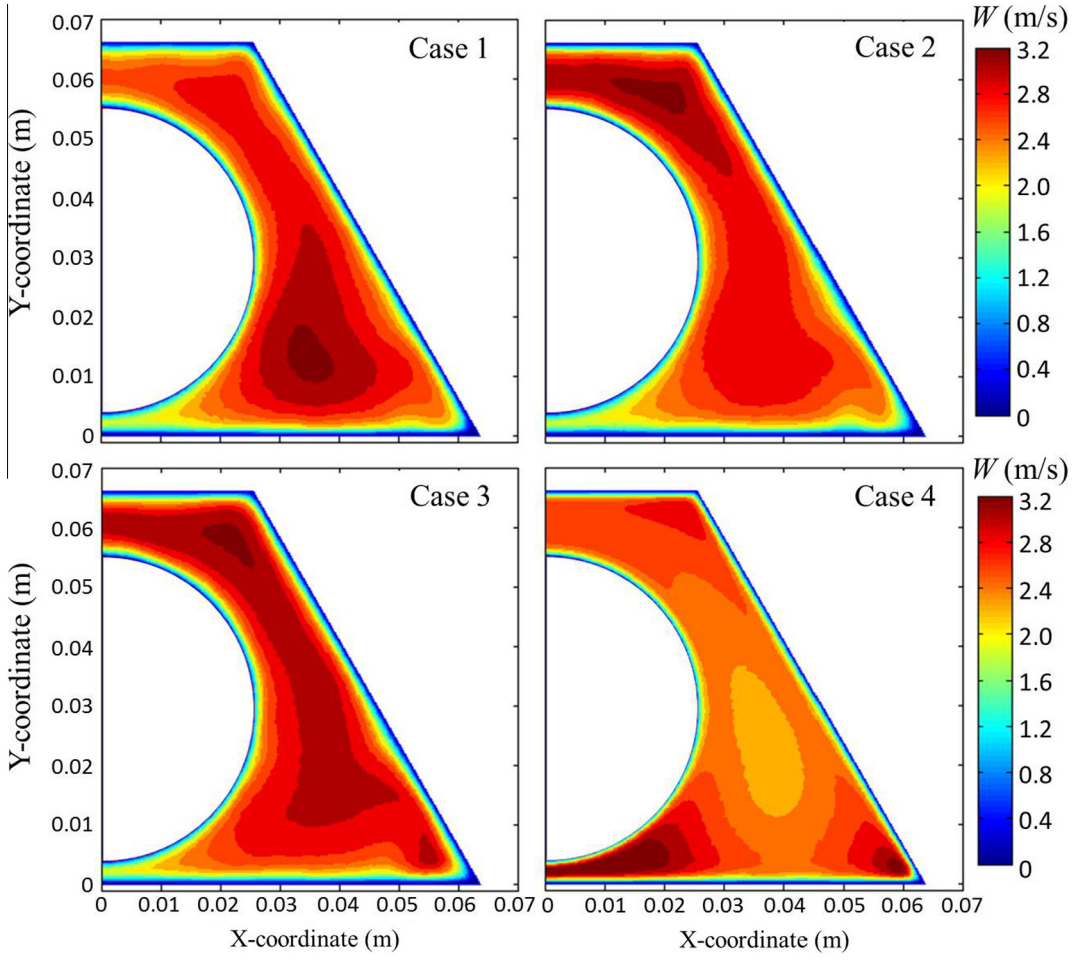

Fig. 6. Contours of streamwise velocity.

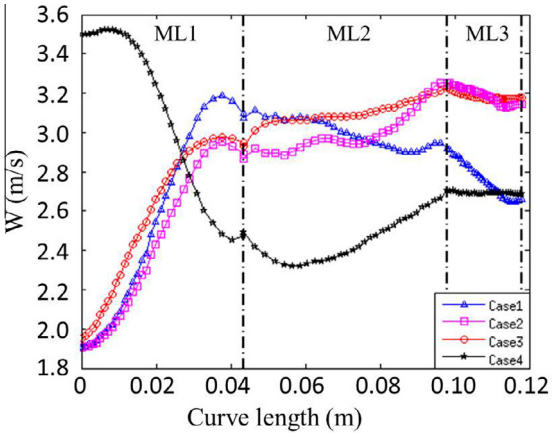

Fig. 7. The velocity magnitude on the equal-distance lines.

in the channel is expected to change the performance of the flow structures, which will be discussed in the following sections.

3.2.2. Instantaneous flow flied and large flow structure

3.2.2.1. Instantaneous velocity field. The general features of the large flow structures in the narrow gap can be visualised via the instantaneous velocity field in the region. The contours of the streamwise velocity at a particular point in the cases are illustrated in Fig. 8. The existence of the swinging large flow structures in the region is clearly shown. It also shows that the wavelengths of the flow structures in each case are not constant but with some jittering, which is agreed with the findings of other authors, seeing Meyer (2010). It is interesting to note that the swinging structure is much weaker in Case 4, while the velocity in the vicinity of the narrow gap is greatly accelerated. The velocity magnitude in the region is even higher than the value in the main channel.

In order to investigate the flow structures with more details, representative time history of normalised fluctuating spanwise velocity (u'/U_b) at 'MP1' and 'MD' are presented in Fig. 9. As shown in Fig. 9(a), there are strong and very regular oscillations of spanwise velocity in the narrow gap in all of the cases. But instantaneous velocity in Case 4 is more irregular than others. The periods of the signals shown in the figure are not perfectly constant, which is consistent with the changing wavelength of the flow structures in the narrow gap mentioned above. Again, the amplitude of the oscillations changes with the change of the buoyancy. It decreases from the value ~30% U_b in Case 1 to ~25% and ~20% U_b in Cases 2 and 3 respectively, but is increases again in Case 4 to ~30% U_b.

The u' at 'MD' shows very weak periodic oscillations with high turbulent noises in Case 1, refer to Fig. 9(b). Such oscillations are hugely suppressed and almost vanish in Case 2, but strengthened in the other two cases, especially in Case 4. It is interesting to note that the dominant periods of u' at 'MD' in Case 4 is quite similar to that at 'MP1'.

Please cite this article in press as: Duan, Y., He, S. Large eddy simulation of a buoyancy-aided flow in a non-uniform channel – Buoyancy effects on large flow structures. Nucl. Eng. Des. (2016), http://dx.doi.org/10.1016/j.nucengdes.2016.05.007

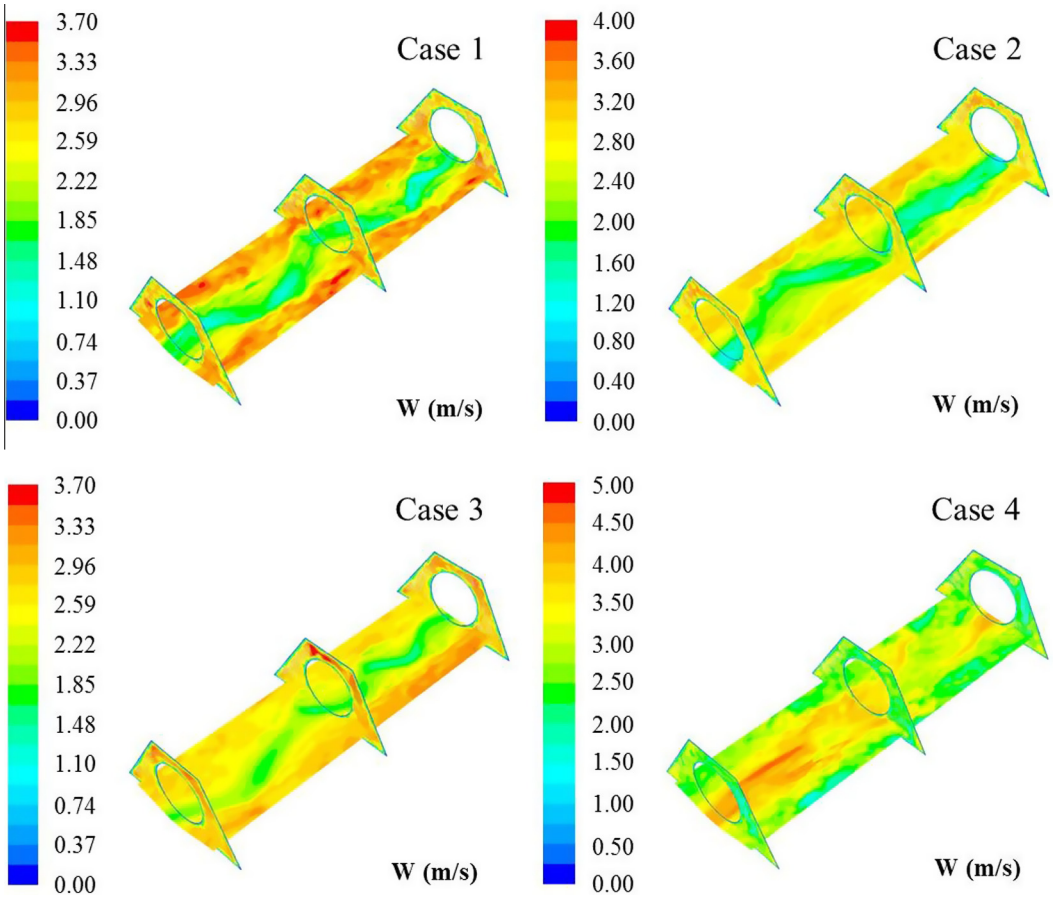

Fig. 8. Contours of streamwise velocity to show the instantaneous flow fields of all of the cases.

3.2.2.2. PSD of fluctuating velocity. It is difficult to determine the exact values of the dominant frequency of the flow structures just by studying the instantaneous velocity history. The power spectra densities (PSD) of the u' at the position 'MP1' and 'MD', shown in Fig. 10, are discussed here to obtain the dominant frequency of the large flow structures and the buoyancy effect on it. To facilitate the comparison between the results from different cases, the original results from Cases 1, 2, 3 and 4 are multiplied by a factor of 10^0, 10^2, 10^4 and 10^6 respectively. The power spectral densities of u'are noted as 'PSDX' while 'f_p' stands for the peak/dominant frequency in the PSDX in the following discussion.

Similar to the results of experimental work done by Wu and Trupp (1993), the pronounced peak in PSDX is not only found at the centre of the narrow gap ('MP1'), but also at the centre of the wide gap ('MD') in the various cases. This again indicates the existence of large flow structures in the wide gap. In terms of PSDX at 'MP1', it is also interesting to note that there are secondary peaks located at either side of the dominant peaks in all the cases, except for Case 4. This suggests that the coherent flow structures in the narrow gap are complicated and there are multi-scales structures under the conditions considered in this research. The f_p of u' at 'MD' in Cases 1, 2 and 3 is every similar to the frequency of the sub-peak located at the left of the dominant peak at 'MP1'. In particular, the peak frequency of u' at 'MD' in Case 4 is the same as that at 'MP1'. It is reasonable to infer that the structures in the narrow gap and wide gap are strongly correlated in Case 4.

The f_p of PSDX at 'MP1' and 'MD' in all cases are listed in Table 1. In Cases 1 and 2 such peak frequencies at 'MP1' are very close to each other (14.0 Hz and 13.7 Hz, respectively), while they are increased in Case 3 (~20.75 Hz), but decreased in Case 4 (~7.32 Hz). The value of f_p remains the same with the location moving away from the centre of the narrow gap such as 'MP2', 'MP3' or even 'MP4'. It is worth to note that there is a big increase in f_p from 'MP3' to 'MP4' in Case 4, which implies a decreased size in the flow structure in the region. The f_p of u' at 'MD' was changed little under the influence of buoyancy force, although the general trend is the same as that at 'MP1'. The highest PSDX at 'MD' is 9.16 Hz in Case 3. The smallest is 7.32 Hz in Case 4. The values in Cases 1 and 2 are 8.55 Hz and 7.93 Hz.

In the current study, the St^{-1} evaluated using u_τ in Case 1 is 0.3787, which is about double the value (0.16) of the experiment of Wu and Trupp (1993) for the same geometry configuration. However, the $St_b{}^{-1}$ evaluated using the bulk velocity is 5.57, which is very close to the experimental value of 5.20. A possible reason for this inconsistency is that the relationship between the friction velocity and *Re* number is not linear. It also suggests that the *St* is better correlated with U_b than with u_τ. To avoid confusion, the *St* used in the following discussion is defined as $f_p D_h/U_b$. The relationship between $St^{-1}/St_f{}^{-1}$ and buoyancy parameter Bo^* is shown in Fig. 11. Here, *St* is the Strouhal number in buoyancy influenced cases and St_f is from Case 1. When the buoyancy force is small, the St^{-1} decrease with the increase of heat flux, see the values of $St^{-1}/St_f{}^{-1}$ in Cases 2 and 3. The trend changes once the heat flux is sufficiently high. It can be seen in the figure that the value of St^{-1} is greatly increased in Case 4. The value of St^{-1} of the flow structures in the wide gap follows the same trend, although the response of St^{-1} to the change of Bo^* is more moderate. It is interesting to point out that the relationship between St^{-1} and Bo^* is similar to the relationship of *Nu* and Bo^* in the buoyancy aiding mixed convection. There is a critical Bo^*, Bo_0^*. The St^{-1} decreases

Please cite this article in press as: Duan, Y., He, S. Large eddy simulation of a buoyancy-aided flow in a non-uniform channel – Buoyancy effects on large flow structures. Nucl. Eng. Des. (2016), http://dx.doi.org/10.1016/j.nucengdes.2016.05.007

with the increase of Bo^*, when $Bo^* < Bo_0^*$. However, it recovers or even increases once $Bo^* > Bo_0^*$.

The relationship between the flow structures in the narrow and wide gaps is further studied using cross correlation functions of u' between 'MP1' and 'MD', which is shown in Fig. 12. As illustrated in the figure, u' at 'MP1' is correlated with that at 'MD' in all of the cases, and, the correlation in Case 4 is much stronger than in the other cases. Especially, it is noticed that the maximum correlation in Case 4 is with 0 s lag, while it is not the case in the other three cases. Together with the fact that the same f_p of the flow structure is observed at 'MP1' and 'MD' in Case 4, it reasonable to conclude that the flow structures passing the wide gap and the narrow gap in Case 4 are closely connected with each other.

The velocity is redistributed across the flow domain under the influence of the non-uniformly distributed body force. A high velocity patch is first formed in the wide gap in the channel when the heat flux is small. It moves towards the narrow gap with the increase of the heat flux. The shape of the velocity profile in the narrow gap region change significantly with the increase of buoyancy parameter Bo^*. A 'V' shape velocity profile is resulted when $Bo^* < Bo_0^*$. The velocity is lowest at the centre of the gap, increasing with the distance away from it, see Fig. 13(a). When $Bo^* > Bo_0^*$, the velocity profile changes to a 'Λ' shape; the velocity is higher in the narrow gap but lower in the main channel, see Fig. 13(b). The flow structure in the low Bo cases, i.e., the 'V' velocity profile in the narrow gap, can be explained by the theory suggested by Krauss and Meyer (1998). The flow structures in the narrow gap are formed by two streets of counter-rotating vortex, which are dependent on the velocity gradient in the region and fuelled by the high velocity in the main channel. The vortices rotate towards the narrow gap, see Fig. 13(a). Once $Bo^* > Bo_0^*$, (i.e., in the strongly buoyancy-influenced cases), the velocity profile changes from

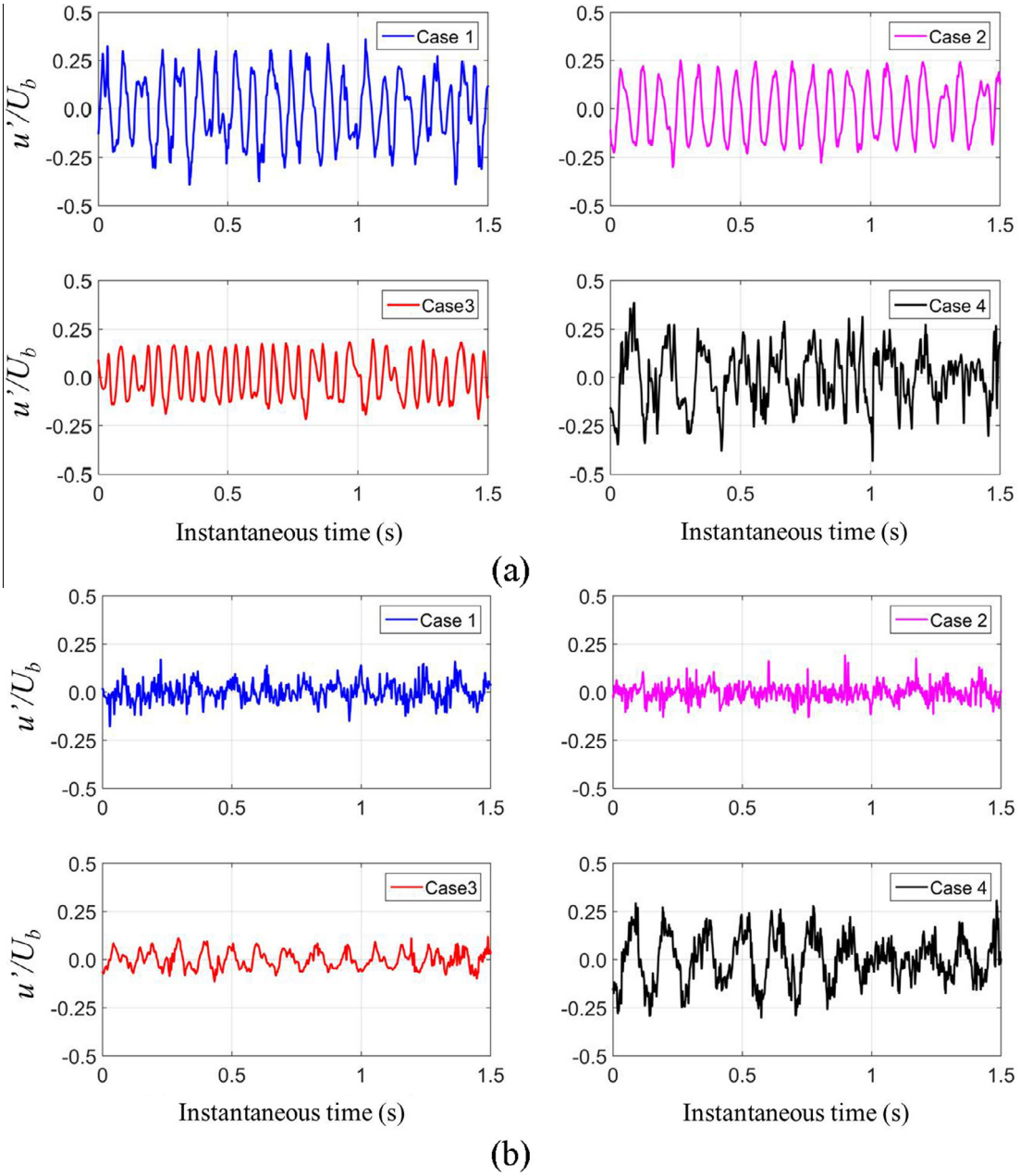

Fig. 9. The ratio u'/U_b at (a) 'MP1'; (b) 'MD' in the cases.

Please cite this article in press as: Duan, Y., He, S. Large eddy simulation of a buoyancy-aided flow in a non-uniform channel – Buoyancy effects on large flow structures. Nucl. Eng. Des. (2016), http://dx.doi.org/10.1016/j.nucengdes.2016.05.007

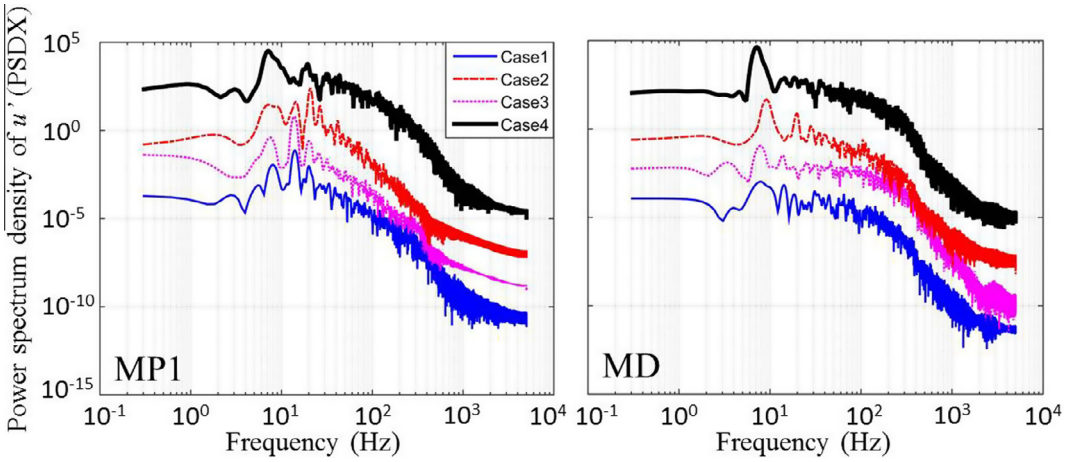

Fig. 10. Power spectral density of the u′ (PSDX) at 'MP1' and 'MD' in all of the cases. The results of Cases 2, 3 and 4 are multiplied by a factor of 10^2, 10^4 and 10^6, respectively.

Table 1
The frequencies (Hz) of the peaks in the power spectrum density of u′ at selected locations.

Locations	Case 1	Case 2	Case 3	Case 4
MP1	14 Hz	13.7 Hz	20.75 Hz	7.32 Hz
MP2	14 Hz	13.7 Hz	20.75 Hz	7.32 Hz
MP3	14 Hz	13.7 Hz	20.75 Hz	7.63 Hz
MP4	14 Hz	13.7 Hz	20.75 Hz	20.14 Hz
MD	8.55 Hz	7.93 Hz	9.16 Hz	7.32 Hz

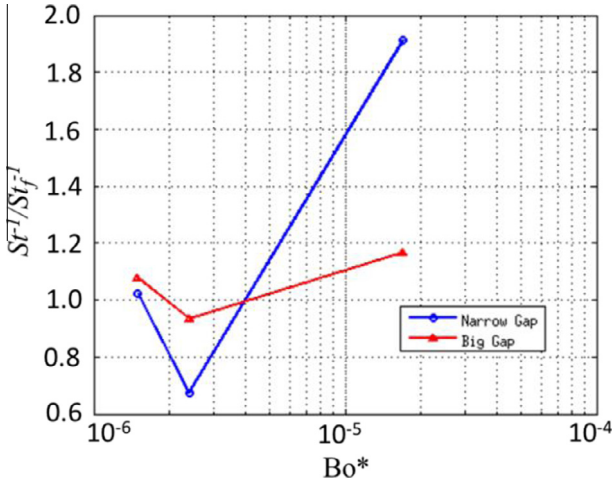

Fig. 11. Ratio of $St^{-1}$of buoyancy influenced cases over St_f^{-1} of the forced convection case.

shape 'V' to 'Λ'. It is reasonable to assume that the two streets of vortices at either side of the narrow gap will likely rotate outwards the narrow gap as illustrated in Fig. 13(b).

3.3. The size of the flow structures

Since the large flow structures are mostly related to 'cross flows' between the various sub-channels, the horizontal fluctuating velocity u' is a good quantity to describe the flow behaviours as shown earlier. The scale of such flow structures can be statistically measured using two-point correlation (Pope, 2000; Home and Lightstone, 2014). The spanwise scale of the large flow structures in the narrow gap is studied using the cross-correlations of u' between 'MP1' and the other 30 points along 'ML1', while the axial scale of the dominant flow structures in the narrow/wide gap can be approximated using the cross correlation of u' between the points located axially at 'MP1' and 'MD' down the channel. These results are presented in Figs. 14 and 15.

The spanwise scale of the structure in the narrow gap is almost the same in the first 3 cases (see Fig. 14), while a visible reduction can be seen in Case 4. As shown in Fig. 15(a), the axial scale of the large flow structures in the narrow gap is about the same in Cases 1 and 2, but is significantly smaller in Case 3, and significantly bigger in Case 4. In the latter, the size is around the size of the domain according to the correlation. The axial scales of the flow structures in the large gap are all similar to each other and are all around the size of the domain, see Fig. 15(b).

When the length scale of the flow structures are similar to, or even greater than, the size of the domain, the above correlation approach is no longer appropriate and an alternative method will have to be used to estimate the scales. It was suggested in Guellouz and Tavoularis (2001a) and Chang and Tavoularis (2012) that the streamwise spacing of the flow structures can be estimated using a convective velocity (U_c) and the dominant frequency (f_p), while the U_c of the flow structures is calculated as the ratio of streamwise distance and time delay of the maximum correlation between two axially aligned points. Space–time correlations can be used to determine the convection velocity and dominant frequency of flow structures. Several points close to the inlet boundary are selected for such a purpose. The point at 0.07 m down the channel in the centre of the gaps is chosen as the reference. Fig. 16 is a representative plot of the streamwise space–time correlation of u' in the centre of the narrow gap as a function of time delays, whereas Fig. 17 shows that in the centre of the wide gap.

The calculated convection velocity and dominated wavelength of the flow structures in the narrow gap and wide gap are listed in the Table 2. The wavelength is calculated using the equation U_c/f_p. The U_c of the large flow structures in the narrow gap remains similar (~2.16 m/s) in the Cases 1, 2 and 3, but is more than 50% higher in Case 4 (~3.31 m/s). This trend is similar to the change of the velocity magnitude in the centre of narrow gap, which also suggests that the U_c is likely to be correlated with the averaged velocity in the region. Considering the calculated axial scale of flow structures in the narrow gap, it decreases from 5 D_h in Cases 1 and 2 to 3.33 D_h in Case 3, which is consistent with the observations in Fig. 15. Due to the increased U_c together with the almost halved f_p (in comparison with Case 1), the wavelength in Case 4 is greatly increased to ~14 D_h. The U_c of large flow structures in the wider gap in Cases 1 and 4 are smaller than in Cases 2 and 3.

Please cite this article in press as: Duan, Y., He, S. Large eddy simulation of a buoyancy-aided flow in a non-uniform channel – Buoyancy effects on large flow structures. Nucl. Eng. Des. (2016), http://dx.doi.org/10.1016/j.nucengdes.2016.05.007

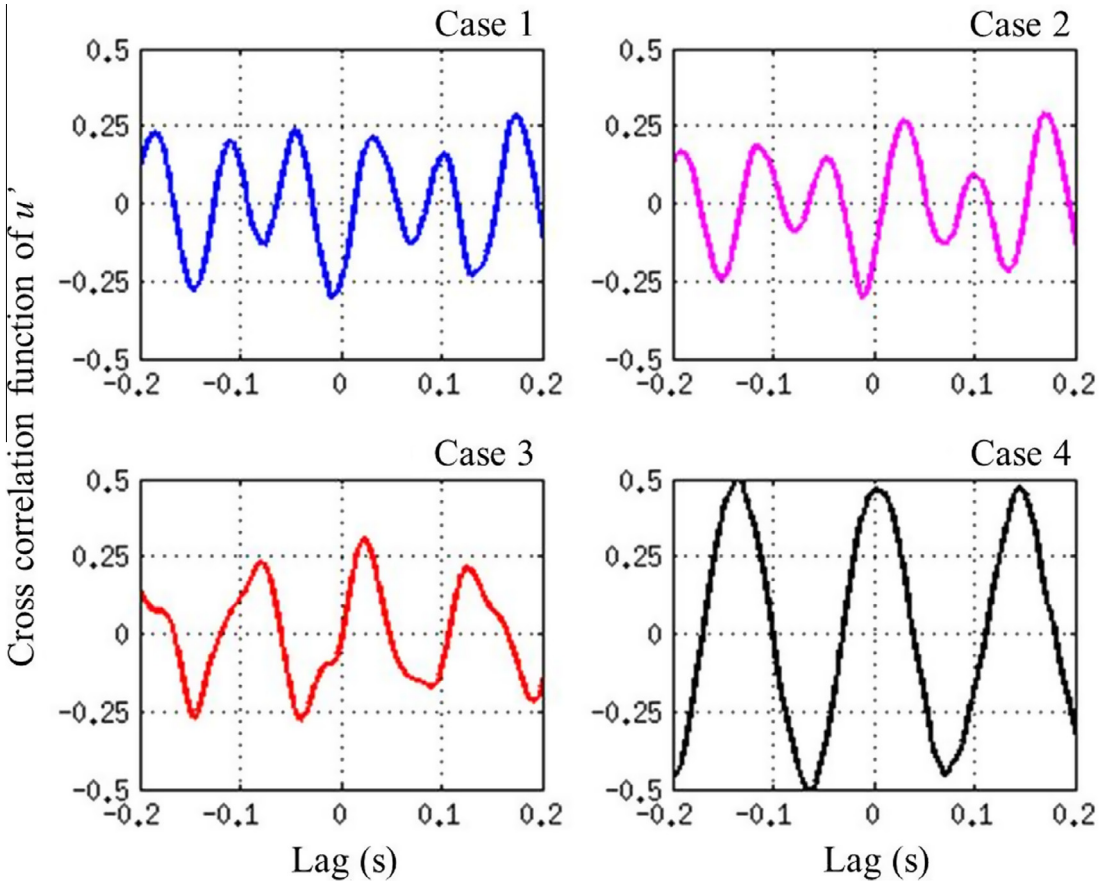

Fig. 12. The cross correlation function of u' between 'MP1' and 'MD'.

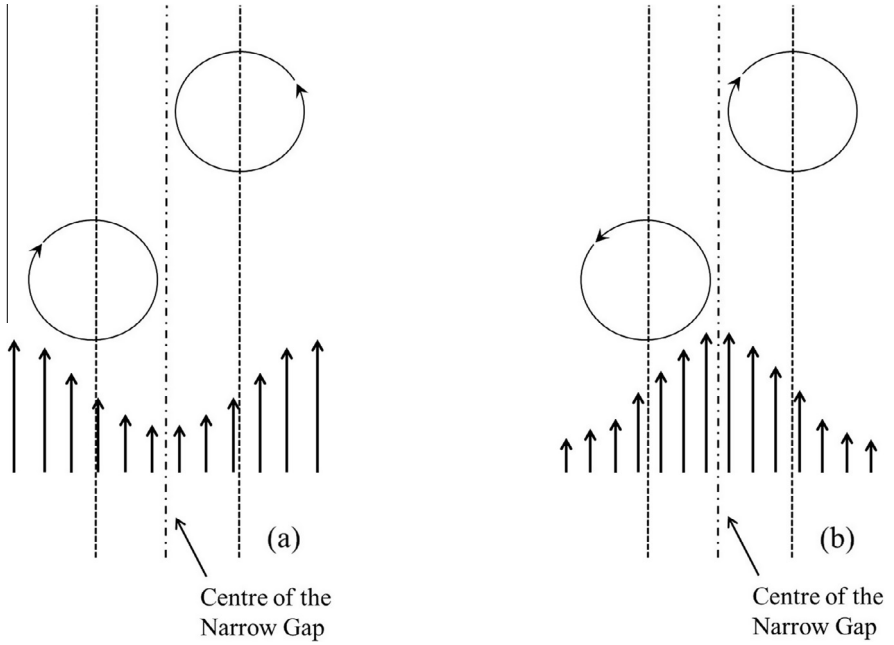

Fig. 13. Flow model of the turbulent vortices in the narrow gap (a) low buoyancy flow; (b) high buoyancy flow.

Furthermore, the general buoyancy effect on the axial scale of the flow structures in the wide gap is similar to those in the narrow gap. The streamwise spacing decreases in Case 3 but recovers in Case 4 in comparison with that in Case 2. The only difference is that the length scale is increased visibly from 9.3 D_h in Case 1 to 11.5 D_h in Case 2.

Please cite this article in press as: Duan, Y., He, S. Large eddy simulation of a buoyancy-aided flow in a non-uniform channel – Buoyancy effects on large flow structures. Nucl. Eng. Des. (2016), http://dx.doi.org/10.1016/j.nucengdes.2016.05.007

3.4. Mixing factor

Due to the existence of the flow structures, the turbulence mixing between the two sides of the narrow gap is enhanced. It is useful to investigate the mixing factor due to the large flow structures. The mixing factor can be evaluated by the equation introduced by Rehme (1992) shown below

$$Y = \frac{u_{eff}\delta_{ij}}{\bar{\varepsilon}} \tag{2}$$

where δ_{ij} is the distance between the sub-channels, the value of which value is taken as 0.09 m the same as that adopted by Wu and Trupp (1994). u_{eff} and $\bar{\varepsilon}$ are the effective mixing velocity and reference eddy viscosity, which are evaluated by the following equations used by Wu and Trupp (1994):

$$u_{eff} = \sqrt{\int_{f_p-\frac{f_p}{4}}^{f_p+\frac{f_p}{4}} E_{uu}(f)df} \tag{3}$$

where f_p is the peak frequency in the power spectra density, $E_{uu}(f)$ the power spectra density function, and,

$$\bar{\varepsilon} = 0.0177 v Re\sqrt{f_t} \tag{4}$$

where v is the kinematic viscosity and f_t is the friction factor defined as $f_{pipe}/8$. The value of f_t is 0.03712, which is converted from the pipe flow with similar Reynolds number, refers to You et al. (2003). So $\bar{\varepsilon}$ is $2.6 * 10^{-4}$.

The value of u_{eff} obtained at 'MP1' ($x/\delta_{ij} = 0$) and other two locations 'MP2' ($x/\delta_{ij} = 0.08$) and 'MP3' ($x/\delta_{ij} = 0.18$) are documented in Table 3. It is really interesting to see that u_{eff} at the 'MP1' in Case 1 is 0.331 which is very similar to the value of 0.34, published by Wu and Trupp (1994), even though the *Re* in their work is ten times higher than in here. With the location away from the centre of the narrow gap, u_{eff} decreases. This is consistence with the finding by Möller (1992). The decreases can be explained by the decreased peak power spectra values. The values in the table also clearly indicate that u_{eff} at all of the locations decreases with the increase of the buoyancy force.

Meanwhile, u_{eff} is usually calculated away from the centre, at the location $x/\delta_{ij} = 0.2$ as proposed by Rehme (1992). Most available spectral density data are located at the centre of the narrow gap. A correlation was suggested by Rehme (1992) to evaluate the u_{eff} at the location away from the centre of the narrow gap between the rod and channel wall:

$$u_{eff} = u_{eff,x=0} 10^{-0.78((S/D)-1)^{-0.33}(x/\delta_{ij})} \tag{5}$$

The u_{eff} calculated using Eq. (4) and that of LES are also listed in Table 3. Rehme's correlation can predict the u_{eff} away from the centre of narrow gap with reasonable accuracy. As shown in Fig. 18, at 'MP2' ($x/\delta_{ij} = 0.08$) the ratio between the prediction of correlation and simulation is around 0.85. With the location moving further away to 'MP3' the accuracy of the correlation is more likely to be affected by the buoyancy force. The ratio varies from 0.752 to 1.26 at 'MP3'. The change in the spanwise size of the flow structures in the narrow gap due to buoyancy force is expected to be one of the reasons.

Since the sub-channels are connected with each other through the symmetric plane of the geometry the mixing factors *Y* of different cases are evaluated using u_{eff} at the centre of narrow gap, which are listed in the Table 4. The value of *Y* for the forced convection (Case 1) is 113.5. It is about 7.5 times the value of 15.4 shown in the article by Wu and Trupp (1994). This is not surprising because u_{eff} is about the same in the current study and in Wu and Trupp (1994) but $\bar{\varepsilon}$ is significant lower in the present study due to the reduction of the Reynolds number. The value of *Y* decreases with the increase of the buoyancy force, as the

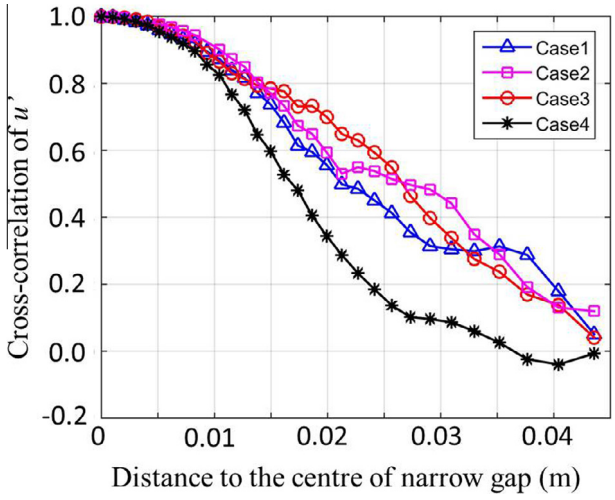

Fig. 14. Cross correlation of u' at the centre of the narrow gap and various points along the line 'ML1'.

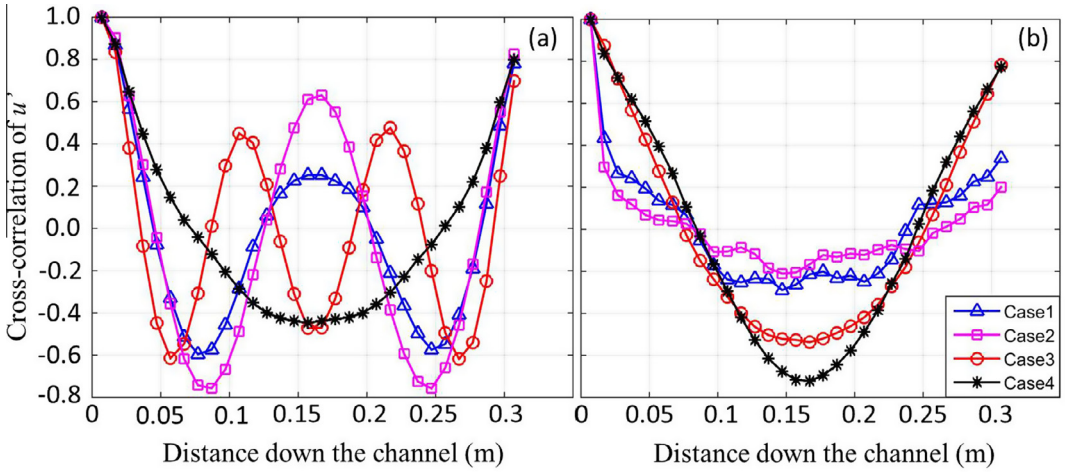

Fig. 15. Cross correlation of u' at different axial points located in the middle of (a) narrow gap and (b) wide gap.

Please cite this article in press as: Duan, Y., He, S. Large eddy simulation of a buoyancy-aided flow in a non-uniform channel – Buoyancy effects on large flow structures. Nucl. Eng. Des. (2016), http://dx.doi.org/10.1016/j.nucengdes.2016.05.007

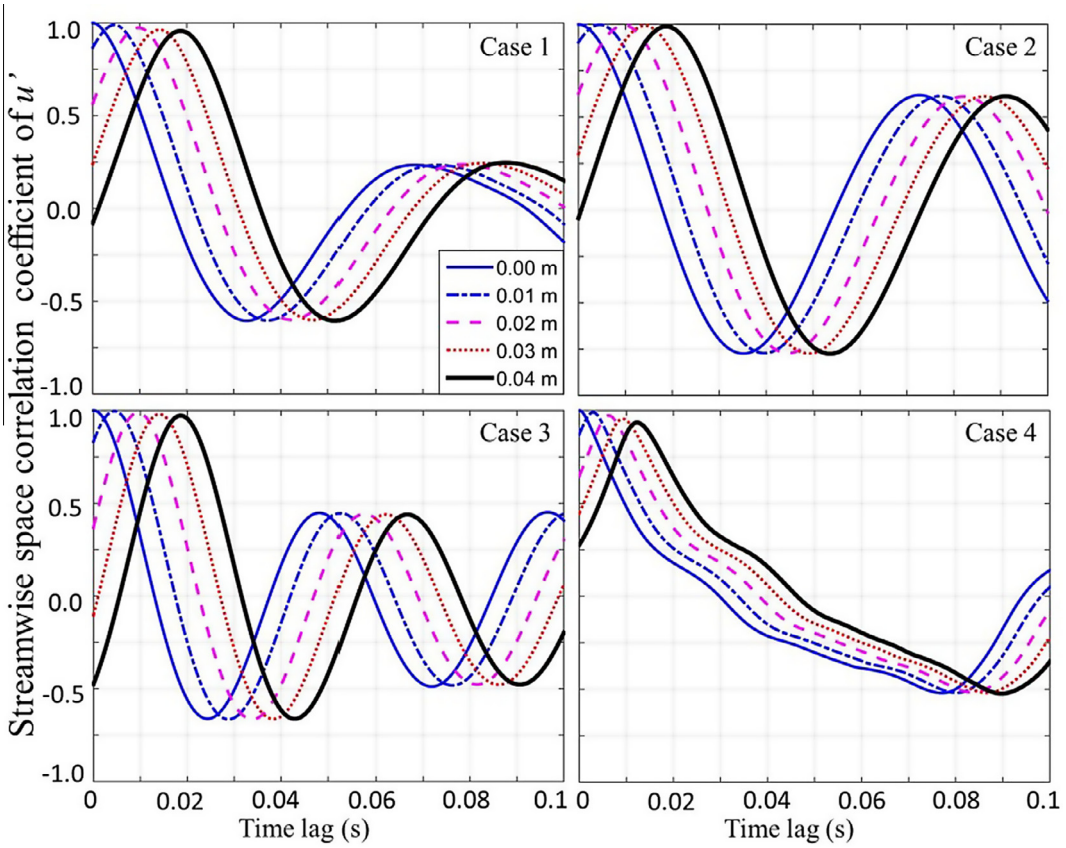

Fig. 16. The streamwise space–time correlation function of u' between point at 0.07 m and other points down the channel at centre of narrow gap in all of the cases. (The value in the legend shows the distance of the point away from the reference point $z = 0.07$ m.)

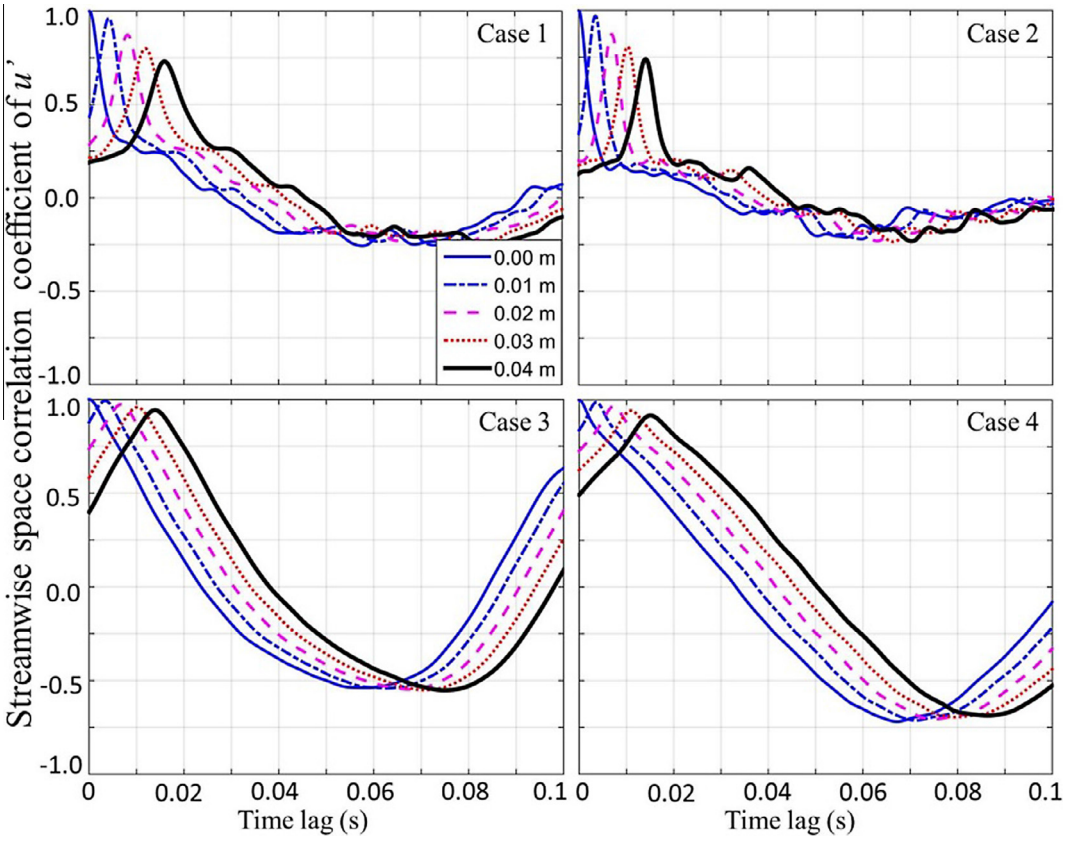

Fig. 17. The streamwise space–time correlation function of u' between point at 0.07 m and other points down the channel at centre of wide gap in all of the cases. (The value in the legend shows the distance of the point away from the reference point $z = 0.07$ m.)

Please cite this article in press as: Duan, Y., He, S. Large eddy simulation of a buoyancy-aided flow in a non-uniform channel – Buoyancy effects on large flow structures. Nucl. Eng. Des. (2016), http://dx.doi.org/10.1016/j.nucengdes.2016.05.007

Table 2
The convection velocity and wavelength of flow structures in narrow gap and bigger gap.

	Narrow gap		Wide gap	
	Convection velocity (m/s)	Wave length/Dh	Convection velocity (m/s)	Wave length/Dh
Case 1	2.159	4.912	2.488	9.267
Case 2	2.156	5.013	2.857	11.473
Case 3	2.176	3.339	2.913	10.127
Case 4	3.313	14.412	2.689	11.697

Note: '*Dh*' is the hydraulic diameter of the considered channel.

Table 3
u_{eff} at certain locations and the ratio between values calculated from simulation and correlation.

Cases	u_{eff} from LES			u_{eff} calculated using Eq. (5)	
	$x/\delta_{ij} = 0$	$x/\delta_{ij} = 0.08$	$x/\delta_{ij} = 0.18$	$x/\delta_{ij} = 0.08$	$x/\delta_{ij} = 0.18$
1	0.331	0.268	0.178	0.237	0.157
2	0.327	0.272	0.17	0.234	0.155
3	0.206	0.182	0.13	0.148	0.098
4	0.199	0.17	0.075	0.143	0.094

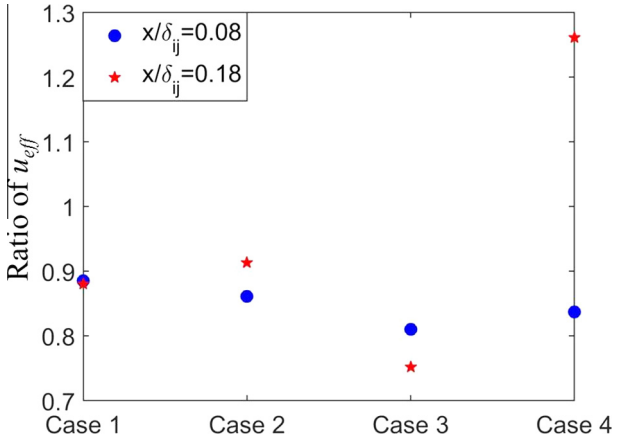

Fig. 18. The ratio of u_{eff} evaluated by Eq. (5) and LES from different cases.

Table 4
Mixing factor of cases.

Cases	Y	Y/Y_f
1	113.50	1
2	112.04	0.987
3	70.692	0.623
4	68.224	0.601

Note: Y_f is the Y of the forced convection case (Case 1).

u_{eff} decreases. It decreases rapidly when the Bo^* increases from 1.5×10^{-6} to 2.4×10^{-6} in Cases 2 and 3, while the value is about the same in the Cases 3 and 4.

4. Conclusions

The buoyancy-aided flow in a heated non-uniform flow passage with a constant wall temperature is studied using large eddy simulation (LES) with a wall adapting local eddy viscosity (WALE) model. The wall temperature is varied in different cases to study the effect of buoyancy. The quality of the simulations is demonstrated by using the LES criteria suggested by Geurts and Fröhlich (2002) and Celik et al. (2005). The main objective of this research is to study the effect of buoyancy force on the flow structures. The key conclusions are summarised below.

The numerical model accurately predicts the behaviours of the flow structures under the isothermal condition. In particular the St^{-1} of the flow structures based on the bulk velocity is very close to that obtained in the experimental work, even though the Reynolds number of the present cases is just 10% of the original experiments. It again proves that the St is dependent on the geometric configuration only. In agreement with the findings of Wu and Trupp (1993), the present numerical simulation also demonstrates that the large flow structures do not just exist in the narrow gap of the flow passage but also in the wide gap.

Due to the non-uniform distribution of body force, the velocity field can be modified due to the buoyancy force. The velocity in the narrow gap may be even higher than in the main channel when the buoyancy force is sufficiently strong. As a result, the formation of the large flow structures may be significantly modified. In addition, some effects of the buoyancy force on the large flow structures in the vicinity of the narrow gap are quite similar to its effect on the general turbulence. The flow structures in the region are suppressed when heat flux is applied. The amplitude of the velocity oscillations decreases together with a reduced wavelength as well as a decreased St^{-1}. Once the heat flux is sufficiently high, the amplitude of the velocity oscillations recovers, the flow structures are stretched and St^{-1} becoming bigger. The effect of buoyancy on the large flow structures in the wide gap is a little different. The oscillation of the velocity due to the flow structures is weak in a forced convection flow. However, the oscillation of the velocity is enhanced once the heat flux is sufficiently high. The strengthened correlation between the flow structures in the narrow gap and wide gap is the main reason. The influence of Bo^* on St^{-1} in the wide gap is similar to its counterpart in the narrow gap.

The mixing factor due to the large flow structures in the narrow gap has also been discussed. It is demonstrated that the effective mixing velocity u_{eff} in the present forced convection case is similar to the value obtained by Wu and Trupp (1994), even though the Reynolds number of the flow they considered is ten times that of the current flow. The buoyancy force reduces the u_{eff} and results in a reduced mixing factor. Finally, it has been demonstrated that the correction of Rehme (1992) of the u_{eff} profile in the gap predicts the results of the present cases well, including the flows with buoyancy influences.

Acknowledgements

The authors would like to acknowledge the financial support provided by EDF Energy as well as the support of the EPSRC UK Turbulence Consortium (grant no. EP/L000261/1), which provides access to the facilities of the UK national supercomputer ARCHER.

Appendix A

By considering the gird resolution and the Kolmogorov length scale, Celik et al. (2005) proposed another quality index for the large eddy simulation:

$$\text{LES\_}IQ_v = \frac{1}{1 + \alpha_v \left(\frac{s^*}{1-s^*}\right)^n} \tag{A.1}$$

where $\alpha_v \simeq 0.05$ and $n \simeq 0.53$. When LES_IQ_v is larger than 0.8, the LES is normally considered as good, when it is equal or above 95% the simulation can be considered as DNS. The challenge brought by this definition is to find a way to evaluate the numerical

viscosity. Celik et al. (2005) proposed the following equation to evaluate it:

$$\mu_{num} = C_v h \sqrt{k_{num}} \tag{A.2}$$

In Celik et al. (2009), numerical kinetic energy $k_{num}$is defined as a function of SGS kinetic energy k_{sgs} in:

$$k_{num} = C_n r^2 k_{sgs} \tag{A.3}$$

while k_{sgs} is defined as:

$$k_{sgs} = \left(\frac{\mu_{sgs}}{C_v \Delta}\right)^2 \tag{A.4}$$

By substituting Eqs. (A.3) and (A.4) into Eq. (A.2), the relation between v_{num} and v_{sgs} can be established:

$$\frac{\mu_{sgs}}{\mu_{num}} = \sqrt{\frac{1}{C_n}}\left(\frac{\Delta}{h}\right)^2 \tag{A.5}$$

C_n is of order of 1. With $\Delta = h$, it can be concluded as:

$$\mu_{num} \approx \mu_{sgs} \tag{A.6}$$

It should be noted the relationships between μ_{sgs} and μ_{num} mentioned above are the guesses based on different assumptions. They can only be used to show the estimations not the accurate results.

References

Abbasian, F., Yu, S.D., Cao, J., 2010. Large eddy simulation of turbulent axial flow along an array of rods. J. Fluids Eng. 132 (2), 021105.
Baglietto, E., Ninokata, H., 2005. A turbulence model study for simulating flow inside tight lattice rod bundles. Nucl. Eng. Des. 235 (7), 773–784.
Baglietto, E., Ninokata, H., Misawa, T., 2006. CFD and DNS methodologies development for fuel bundle simulations. Nucl. Eng. Des. 236 (14–16), 1503–1510.
Baratto, F., Bailey, S.C.C., Tavoularis, S., 2006. Measurements of frequencies and spatial correlations of coherent structures in rod bundle flows. Nucl. Eng. Des. 236 (17), 1830–1837.
Biemüller, M., Meyer, L., Rehme, K., 1996. Large eddy simulation and measurement of the structure of turbulence in two rectangular channels connected by a gap. Engineering Turbulence Modeling and Experiments, vol. 3, pp. 249–258.
Celik, I.B., Cehreli, Z.N., Yavuz, I., 2005. Index of resolution quality for large eddy simulations. J. Fluids Eng. 127 (5), 949–958.
Celik, I., Klein, M., Janicka, J., 2009. Assessment measures for engineering LES applications. J. Fluids Eng. 131 (3), 031102.
Chang, D., Tavoularis, S., 2005. Unsteady numerical simulations of turbulence and coherent structures in axial flow near a narrow gap. J. Fluids Eng. 127 (3), 458–466.
Chang, D., Tavoularis, S., 2006. Convective heat transfer in turbulent hlow near a gap. J. Heat Transfer 128 (7), 701–708.
Chang, D., Tavoularis, S., 2007. Numerical simulation of turbulent flow in a 37-rod bundle. Nucl. Eng. Des. 237 (6), 575–590.
Chang, D., Tavoularis, S., 2008. Simulations of turbulence, heat transfer and mixing across narrow gaps between rod-bundle subchannels. Nucl. Eng. Des. 238 (1), 109–123.
Chang, D., Tavoularis, S., 2012. Numerical simulations of developing flow and vortex street in a rectangular channel with a cylindrical core. Nucl. Eng. Des. 243, 176–199.
Choueiri, G.H., Tavoularis, S., 2014. Experimental investigation of flow development and gap vortex street in an eccentric annular channel. Part 1. Overview of the flow structure. J. Fluid Mech. 752, 521–542.
Fluent, A., 2009. Theory Guide. ANSYS Inc.
Forooghi, P., Abdi, I.A., Dahari, M., Hooman, K., 2015. Buoyancy induced heat transfer deterioration in vertical concentric and eccentric annuli. Int. J. Heat Mass Transfer 81, 222–233.
Geurts, B.J., Fröhlich, J., 2002. A framework for predicting accuracy limitations in large-eddy simulation. Phys. Fluids 14 (6), L41–L44.
Gosset, A., Tavoularis, S., 2006. Laminar flow instability in a rectangular channel with a cylindrical core. Phys. Fluids 18 (4), 044108.
Guellouz, M.S., Tavoularis, S., 1992. Heat transfer in rod bundle subchannels with varying rod-wall proximity. Nucl. Eng. Des. 132, 351–366.
Guellouz, M.S., Tavoularis, S., 2000a. The structure of turbulent flow in a rectangular channel containing a cylindrical rod – Part 1: Reynolds-averaged measurements. Exp. Thermal Fluid Sci. 23 (1–2), 59–73.
Guellouz, M.S., Tavoularis, S., 2000b. The structure of turbulent flow in a rectangular channel containing a cylindrical rod – Part 2: phase-averaged measurements. Exp. Thermal Fluid Sci. 23 (1–2), 75–91.
Home, D., Arvanitis, G., Lightstone, M.F., Hamed, M.S., 2009. Simulation of flow pulsations in a twin rectangular sub-channel geometry using unsteady Reynolds averaged Navier–Stokes modelling. Nucl. Eng. Des. 239 (12), 2964–2980.
Home, D., Lightstone, M.F., 2014. Numerical investigation of quasi-periodic flow and vortex structure in a twin rectangular subchannel geometry using detached eddy simulation. Nucl. Eng. Des. 270, 1–20.
Hooper, J.D., Rehme, K., 1984. Large-scale structural effects in developed turbulent flow through closely-spaced rod arrays. J. Fluid Mech. 145, 305–337.
In, W.K., Shin, C.H., Oh, D.S., Chun, T.H., 2004. Numerical analysis of the turbulent flow and heat transfer in a heated tod bundle. J. Korean Nucl. Soc. 36, 153–164.
Jackson, J.D., Cotton, M.A., Axcell, B.P., 1989. Studies of mixed convection in vertical tubes. Int. J. Heat Fluid Flow 10 (1), 2–15.
Kasagi, N., Nishimura, M., 1997. Direct numerical simulation of combined forced and natural turbulent convection in a vertical plane channel. Int. J. Heat Fluid Flow 18 (1), 88–99.
Keshmiri, A., Cotton, M.A., Addad, Y., Laurence, D., 2012. Turbulence models and large eddy simulations applied to ascending mixed convection flows. Flow Turbul. Combust. 89 (3), 407–434.
Krauss, T., Meyer, L., 1996. Characteristics of turbulent velocity and temperature in a wall channel of a heated rod bundle. Exp. Thermal Fluid Sci. 12, 75–86.
Krauss, T., Meyer, L., 1998. Experimental investigation of turbulent transport of momentum and energy in a heated rod bundle. Nucl. Eng. Des. 180 (3), 185–206.
Liu, M., Ishiwatari, Y., 2011. Unsteady numerical simulations of the single-phase turbulent mixing between two channels connected by a narrow gap. Nucl. Eng. Des. 241 (10), 4194–4205.
Liu, M., Ishiwatari, Y., 2013. Unsteady numerical simulations of single-phase turbulent mixing in tight lattice geometries. Nucl. Eng. Des. 256, 28–37.
Merzari, E., Ninokata, H., 2008. Anisotropic turbulence and coherent structures in eccentric annular channels. Flow Turbul. Combust. 82 (1), 93–120.
Merzari, E., Ninokata, H., 2009. Development of an LES methodology for complex geometries. Nucl. Eng. Technol. 41 (7), 893–906.
Merzari, E., Ninokata, H., Baglietto, E., 2008. Numerical simulation of flows in tight-lattice fuel bundles. Nucl. Eng. Des. 238 (7), 1703–1719.
Merzari, E., Ninokata, H., Mahmood, A., Rohde, M., 2009. Proper orthogonal decomposition of the flow in geometries containing a narrow gap. Theoret. Comput. Fluid Dyn. 23 (5), 333–351.
Meyer, L., 1994. Measurement of turbulent velocity and temperature in axial flow through a heated rod bundle. Nucl. Eng. Des. 146, 71–82.
Meyer, L., 2010. From discovery to recognition of periodic large scale vortices in rod bundles as source of natural mixing between subchannels—a review. Nucl. Eng. Des. 240 (6), 1575–1588.
Meyer, L., Rehme, K., 1994. Large-scale turbulence phenomena compound rectangular channels. Exp. Thermal Fluid Sci. 8, 286–304.
Meyer, L., Rehme, K., 1995. Periodic vortices in flow through channels with longitudinal slots or finx. In: Tenth Symposioum on Turbulent shear flows, The Pensylvania State University, University Park, PA, USA, August 14–16, 1995.
Möller, S.V., 1991. On phenomena of turbulent flow through rod bundles. Exp. Thermal Fluid Sci. 4 (1), 25–35.
Möller, S.V., 1992. Single-phase turbulent mixing in rod bundles. Exp. Thermal Fluid Sci. 5, 26–33.
Ninokata, H., Merzari, E., Khakim, A., 2009. Analysis of low Reynolds number turbulent flow phenomena in nuclear fuel pin subassemblies of tight lattice configuration. Nucl. Eng. Des. 239 (5), 855–866.
Ouma, B.H., Tavoularis, S., 1991. Flow measurements in rod bundle subchannels with varying rod-wall proximity. Nucl. Eng. Des. 131, 193–208.
Patankar, S.V., Liu, C.H., Sparrow, E.M., 1977. Fully developed flow and heat transfer in ducts having streamwise-periodic variations of cross-sectional area. ASME J. Heat Transfer 99, 180–186.
Piller, M., 2005. Direct numerical simulation of turbulent forced convection in a pipe. Int. J. Numer. Methods Fluids 49, 583–602.
Piot, E., Tavoularis, S., 2011. Gap instability of laminar flows in eccentric annular channels. Nucl. Eng. Des. 241 (11), 4615–4620.
Pope, S.B., 2000. Turbulent Flows. Cambridge University Press.
Rehme, K., 1992. The structure of turbulence in rod bundles and the implications on natural mixing between the subchannels. Int. J. Heat Mass Transfer 35 (2), 567–581.
Wu, X., Trupp, A.C., 1993. Experimental study on the unusual turbulence intensity distributions in rod-to-wall gap regions. Exp. Thermal Fluid Sci. 6 (4), 360–370.
Wu, X., Trupp, A.C., 1994. Spectral measurements and mixing correlation in simulated rod bundle subchannels. Int. J. Heat Mass Transfer 37 (8), 1277–1281.
You, J., Yoo, J.Y., Choi, H., 2003. Direct numerical simulation of heated vertical air flows in fully developed turbulent mixed convection. Int. J. Heat Mass Transfer 46 (9), 1613–1627.

Please cite this article in press as: Duan, Y., He, S. Large eddy simulation of a buoyancy-aided flow in a non-uniform channel – Buoyancy effects on large flow structures. Nucl. Eng. Des. (2016), http://dx.doi.org/10.1016/j.nucengdes.2016.05.007